CO Interaction with Small Rhodium Clusters from Density Functional Theory: Spectroscopic Properties and Bonding Analysis

Tzonka Mineva,*,†,|| Nino Russo,‡ and Hans-Joachim Freund§

Institute of Catalysis, Bulgarian Academy of Sciences, bul. G. Bonchev, bl.11, 1113 Sofia, Bulgaria, Dipartimento di Chimica, Universita della Calabria, I-87030 Arcavata di Rende, Italy, and Fritz-Haber Institut der Max-Planck-Gesellschaft, Abteilung Chemische Physik, Faradayweg 4−6, D-14195 Berlin, Germany

Received: May 1, 2001; In Final Form: August 31, 2001

Density functional computations have been performed to determine equilibrium geometrical structures, magnetic properties, and vibrational frequencies of a series of $Rh_x(CO)_y$ ($x \leq 4$, $y \leq 2$) clusters. The results are compared with experiments on CO adsorption on small rhodium aggregates deposited onto a thin, well-ordered alumina film. The CO stretching frequency as a function of rhodium cluster topology and spin-state is reported and discussed. The considered rhodium monocarbonyls are found to exhibit nonzero magnetic moments. They show a more pronounced dependence of the CO-stretching frequency on the magnetic properties than on the number of rhodium atoms. The CO bonding behavior in the formation of $Rh_x(CO)_y$ species is rationalized on the basis of the molecular orbital and the natural bond order analysis.

1. Introduction

The interaction of CO with transition metals and supported metal catalysts has been studied extensively for a long time and, because of its rich chemistry, it is still an important challenge. In the past years, research efforts have also been devoted to nanostructures and nanomaterials. To answer the question of how the catalytic activity and reactivity are affected by the metal−support interaction and by the nanoparticle size, usually the adsorption of small molecules on suitable model systems is undertaken. At the same time, interest in the properties of isolated transition metal clusters, together with their adsorption features, has also become nowadays an active field of research. These studies are expected to give better insight into metal−metal bonds and into transition from gas-phase clusters to solids and to help the development of new materials and catalysts. Recently, the interaction of small Rh_x clusters deposited on a thin alumina film[1,2] with CO molecules was studied utilizing infrared reflection absorption spectroscopy (IRAS).[3−5] In the limit of low metal deposition, remarkably sharp peaks pointed to the presence of uniform isolated particles on the oxide support. This experimental evidence for new type carbonyl species on the thin alumina surface has prompted the current theoretical study.

Theoretical data on CO/Rh species, coming from different levels of computation, have also been reported,[6−14] mainly concerning the geometrical and electronic structures as well as vibrational frequencies of RhCO and $Rh(CO)_2$. The geometrical and vibrational features of $Rh(CO)_3$ and $Rh(CO)_4$ computed by using hybrid and nonlocal functionals within density functional theory (DFT) are also available.[10,11] To our knowledge, there is a limited number of theoretical studies dealing with the interaction of CO with rhodium clusters containing more than two metal atoms.[13,14] In these papers the computations were performed without relaxing the geometry of the metal cluster.

In the present study the computed geometrical and electronic properties and the vibrational frequencies of some $Rh_x(CO)_y$ ($x = 1-4$ and $y = 1,2$) species that are more likely to be relevant to surface chemistry are reported. Following the IRAS data,[3−5] only the atop structures were considered for the Rh_xCO species ($x > 2$). All the calculations were carried out within density functional theory.

Because of the experimental[15−18] and theoretical[19−21] evidence for a nonzero magnetic moment of small Rh_x ($x = 1-13$) clusters, various spin states of the rhodium carbonyls are examined. Thus, the magnetic moment variation of Rh_x upon interaction with carbon monoxide is discussed.

2. Method and Computational Details

Density functional theory in conjunction with the B3LYP[22,23] hybrid exchange correlation functional was employed for the present computations. Rhodium atoms were described using the Los Alamos effective core potential (ECP)[24] plus double-ζ (DZ) quality, and for carbon and oxygen, the 6-311++G** basis set[25] was used. Geometrical parameters of the carbonyl structures were obtained by full optimization with the Berny algorithm,[26] and the calculations were carried out without any constraint on the geometrical parameters. The optimization of the $Rh_3(CO)_y$ and $Rh_4(CO)_y$ structures has led to distortion of the appropriate symmetry group, and therefore the properties of these species were computed without imposing a symmetry constraint.

Vibrational frequencies of the optimized rhodium carbonyl structures were computed by taking finite differences of analytical first derivatives in the framework of the harmonic oscillator approximation.[27] Since the values of the vibrational frequencies are clearly dependent on the methods employed, the properties of CO, RhCO, and $Rh(CO)_2$ are also rationalized by using some different overlaps between the B3LYP functional and all-electron double-ζ (DZVP)[28] basis set for Rh, C, and O and between the Becke-Perdew (BP86) functional[29] and ECP

* Corresponding author: Fax (+359) 2 75 6116; E-mail: tmineva@ic.bas.bg.

† Bulgarian Academy of Sciences.

‡ Universita della Calabria.

§ Fritz-Haber Institut der Max-Planck-Gesellschaft.

|| Presant address: Fritz-Haber Institut der Max-Planck-Gesellschaft, Abteilung Chemische Physik, Faradayweg 4-6, D-14195 Berlin, Germany.

10.1021/jp0116398 CCC: $20.00
Published on Web 11/03/2001

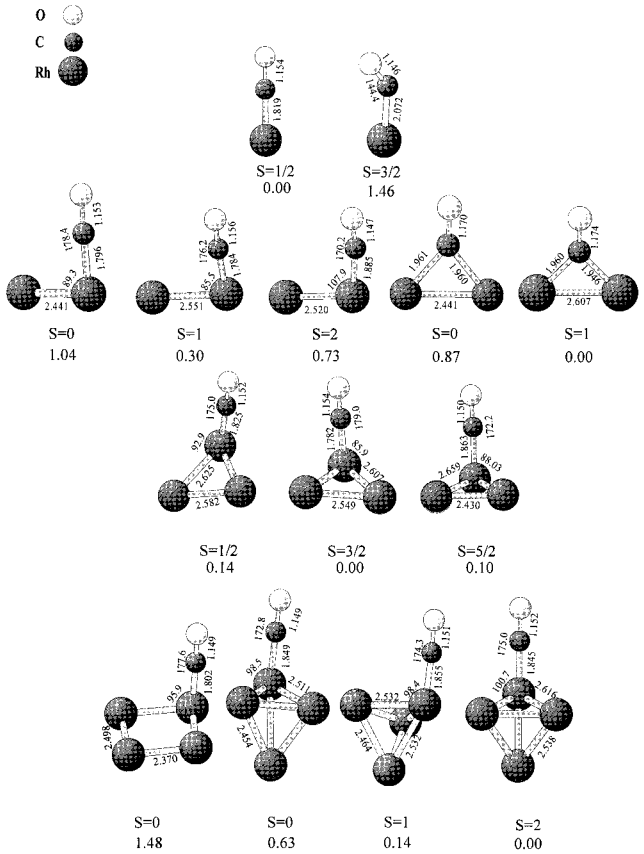

Figure 1. B3LYP-geometrical parameters, total spin, S, and relative energies (eV) for Rh_xCO structures. The bond lengths are in Å and the angles are in degrees.

and all-electron wave functions, respectively. All computations were performed using the Gaussian94 code.[30]

3. Geometrical Parameters, Magnetic Properties, and Potential Energy Surfaces

3.1. Rhodium Monocarbonyls. The B3LYP-equilibrium geometries of rhodium monocarbonyl species (Rh_xCO, $x = 1-4$) with an atop bound CO at different spin states are shown in Figure 1. As seen from the relative energy values reported also in Figure 1, the ground state (GS) for RhCO is found to be a linear molecule with total spin (S) 1/2 and the electronic state $^2\Delta$ in agreement with previous theoretical computations.[7−12] In the case of the rhodium atom, the $^4F(4d^85s^1)$ state is the ground state separated from the first excited $^2D(d^9)$ state by 0.34 eV.[31] The $^4\Delta$ state of RhCO lies 1.46 eV higher in energy and the CO molecule forms an angle of 144.4° with the rhodium atom. In the latter case, the Rh−C distance increases by about 0.25 Å and a slight decrease of the C−O bond is observed. The same tendency has been found also using the complete active space self-consistent field (CASSCF) and multireference singles and doubles configuration interaction (MRSDCI) computational schemes.[8]

For the Rh_2CO species, the linear and bridged CO bonding to the rhodium dimer has been considered. The results in Figure 1 reveal that the most stable structure is the structure with bridging CO and S = 1, followed by the atop Rh_2CO structure with S = 1. The theoretical data for the isolated rhodium dimer refer to the quintet as the GS and the Rh−Rh distance of roughly 2.2 Å.[19−21] Our results show that the interaction of CO with a rhodium dimer leads to a metal−metal bond distance of about 2.5 Å. Hence, the binding of carbon monoxide to Rh_2 causes

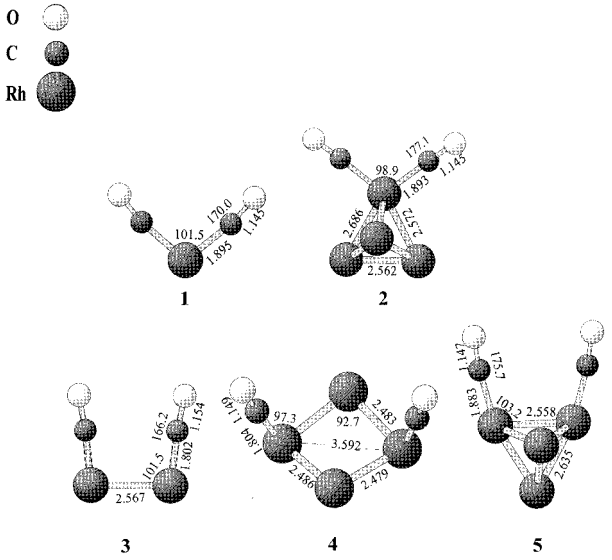

Figure 2. B3LYP-geometrical parameters for $Rh_x(CO)_2$ structures. The bond lengths are in Å and the angles are in degrees.

an increase of the metal−metal bond length and a quenching of the magnetism. The quintet and singlet Rh_2CO clusters with the atop bound carbon monoxide are found to be energetically less stable than the triplet one. In difference to the linearly bound carbon monoxide, a quintet structure with bridging CO was not obtained.

While all previous data agree in predicting a Rh_2 ground state with spin multiplicity 5, there are some controversies about the magnitude of the total spin in the case of Rh_3. The most recent DFT calculations at local[19] and gradient-corrected[19,21] levels of approximation pointed to nearly degenerate quartet and sextet Rh_3 arrangments. This is in agreement with the experimental indications[18] reporting total magnetic moments of 5 or 7 μB. For Rh_3CO, our results give nearly degenerate species with spin 1/2, 3/2, and 5/2. Nevertheless, the quartet structure is found to be lower in energy than the sextet and doublet structures by 0.10 and 0.14 eV, respectively.

From Figure 1, it can be seen that the most stable electronic state of Rh_4CO is that with S = 2, and very close on the potential energy surface (0.14 eV) another structure with S = 1 is found. For Rh_4, the theoretical studies[19−21] predict a paramagnetic ground state with tetrahedral geometry. Experimental works,[18] however, indicate nonzero magnetic moments also for Rh_4 systems. Our computations for the Rh_4CO clearly predict that these species exhibit nonzero magnetic moments. Indeed, the two possible singlet states are found to lie considerably higher in energy (0.63 and 1.48 eV) on the potential energy surface.

The results in Figure 1 reveal no significant changes of Rh−C and C−O bond lengths and Rh−C−O bond angles for the various electronic states of Rh_2CO, Rh_3CO, and Rh_4CO. In fact, only a general tendency of increasing the Rh−C distance by a maximum of 0.1 Å in going from ground to the excited states can be seen. At a higher number of rhodium atoms this effect is even smaller. The linear bonding of the carbon monoxide causes, however, a lengthening of the metal−metal bond ranging up to 0.3 Å in comparison to that in the isolated rhodium clusters.[19−21]

3.2. Rhodium Dicarbonyls. Several possible rhodium dicarbonyls have been studied and their equilibrium structures are depicted in Figure 2. The binding of carbon monoxide molecules to one and two rhodium atoms was considered. The stability of different magnetic states of $Rh_x(CO)_2$ and OC−Rh_x−CO (not shown in Figure 2) has also been examined. For

TABLE 1: Bond Lengths (r) in Å, Mulliken Atomic Charges (q), C−O (ν_{C-O}) Stretching Frequencies in cm^{-1}, and Intensities (I_{C-O}) in km/mol for $RhCO^+$ and $Rh(CO)_2^+$ in Their Ground Electronic States within B3LYP[a]

system (el. state)	r(Rh−C)	r(C−O)	q_{Rh}	q_C	q_O	ν_{C-O}	I_{C-O}
$RhCO^+$ ($^3\Delta$)	2.212	1.117	0.80	0.27	−0.07	2296	115
$Rh(CO)_2^+$ ($^1A_1$)	1.868	1.126	0.49	0.24	0.02	2246	208
						2196	500

[a] The bond angle C−Rh−C = 87.6°.

$Rh(CO)_2$ and OC−Rh_2−CO, the lowest possible spin state is found to be the ground state. The quartet $Rh(CO)_2$ structure lies 2.53 eV above the minimum, and the triplet OC−Rh_2−CO state is 1.22 eV higher in energy than the singlet one. The structures of the $Rh_4(CO)_2$ (structure **2**) and OC−Rh_4−CO (structure **5**) reported in Figure 2 are the triplet ones. The corresponding singlet species are determined to be less stable by 0.14 and 0.23 eV for the $Rh_4(CO)_2$ and OC−Rh_4−CO, respectively. The other considered OC−Rh_4−CO topology (structure **4**) is the singlet one and lies 1.47 eV above structure **5**. The Rh−Rh distances of the $Rh_x(CO)_2$ species are obtained to resemble those of Rh_xCO species. No significant variation of the carbon−oxygen bond length in going from Rh_xCO to $Rh_x(CO)_2$ is obtained either.

3.3. $RhCO^+$ and $Rh(CO)_2^+$. The $RhCO^+$ and $Rh(CO)_2^+$ species were investigated theoretically by numerous authors.[6,7,9−11] We will briefly discuss their geometrical and electronic structures as obtained from the present B3LYP calculations. In Table 1 the bond lengths and angles, together with the electronic state and the Mulliken net charges for the most stable structures, are collected. Our calculations for $RhCO^+$ agree with all previous DF studies,[7,9−11] which predicted the $^3\Delta$ electronic state to be the GS. The ground state of the rhodium cation is also a triplet, $^3F(4d^85s^0)$, and therefore, in contrast to the Rh-atom, the CO interaction with Rh^+ does not lower the spin state. This is not surprising because the spin lowering in the carbonylated metal clusters is attributed to the promotion of the outer s electron into the d shell.[32]

The presence of a second CO molecule results in a singlet GS for $Rh(CO)_2^+$ in agreement with the results obtained by McKee and Worley[9] and Papai et al.[7] The comparison between their Rh−C, C−O, and C−Rh−C values and our data shows very good agreement, notwithstanding the differences in the employed exchange correlation functionals and basis sets. We have examined also the $^3B_2$ state, which is 1.23 eV higher in energy than the GS. This result is in reasonable agreement with the $^1A_1/^3B_2$ energy separation computed by McKee and Worley.[9]

4. Vibrational Frequencies

Infrared spectroscopy is widely used to probe the structure of CO adsorbed on clean metal surfaces and on deposited metal particles in supported catalysts. Theoretical estimates of the vibrational frequencies have already shown to aid a better understanding of the experimental data. The accuracy in the potential energy surface curvature description, which depends on the employed method, affects the absolute value of the vibrational frequency. The use of DF-based approaches, especially for inorganic systems, has led to an improvement in the vibrational frequency computations[33] in comparison to Hartree−Fock theory. Nevertheless, the accumulated results have shown a clear dependence of the vibrational frequency on the choice of the exchange correlation functional and the initial basis sets. To fit the experimental values, scaling factors for the calculated frequencies have been proposed.[34] For these reasons we have examined the variation of the CO stretching frequency (ν_{C-O}) in the free CO, RhCO, and $Rh(CO)_2$ using the nonlocal gradient-corrected BP86 and the hybrid B3LYP functional in conjunction with LANL2 plus DZ for rhodium and 6-311++G** for C and O and DZVP basis sets. These results, together with the bond lengths, bond-angles, and previous MRSDCI[8] and local spin density (LSD)[7] data, are collected in Table 2. The considered electronic states, $^1\Sigma$ for CO, $^2\Delta$ for RhCO, and $^2B_2$ for $Rh(CO)_2$, are those yielding minimum energies for the respective species. The same ground states were indicated by the previous theoretical studies.[7−12,14] The results in Table 2 reveal a good agreement between the different levels of theory for the geometrical structures, while for ν_{C-O} a variation of up to 100 cm^{-1} is observed. Examining the predicted reduction in ν_{C-O} of the free CO in RhCO and $Rh(CO)_2$ species, it is worth noting that the divergence of the various approximations is only 2% for RhCO and 1% for the gem-dicarbonyl. Hence, whichever functional and basis sets within the DFT are employed, the vibrational shift seems to be adequately computed in the framework of the harmonic oscillator approximation.

4.1. CO Stretching Frequencies of Rh_xCO. The CO stretching frequencies of the considered monocarbonyl structures are collected in Table 3. Discussing the ν_{C-O} in the Rh_xCO ground and excited states, it emerges that the GSs of the clusters with an odd number of metal atoms are accompanied by the highest ν_{C-O} values. By contrast, clusters with an even number of Rh atoms show a decrease of ν_{C-O} in going from the excited to the ground states. Although the variation of the CO bond distance with the system multiplicity (see Figure 1) seems to be negligibly small, the dependence of the CO stretching frequency on the magnetic properties results in a shift, e.g., of about 40 cm^{-1} in the Rh_2CO and Rh_4CO clusters.

Usually, the infrared bands in the range of 1950−2070 cm^{-1} are attributed to a single adsorbed CO molecule attached to a single Rh atom, which is thought to be a part of larger particles of supported rhodium atoms.[35] On rhodium single-crystal surfaces, the CO atop adsorption at low coverage is identified through vibrational frequencies[35−37] between 1995 and 2030 cm^{-1}, while the experimental stretching frequency of free CO is 2143 cm^{-1}[38]. The comparison of our GS frequencies with these experimental data shows that even very small rhodium carbonyls can be successfully used for theoretical models of CO interaction with rhodium surfaces or large supported particles. In fact, the B3LYP values of ν_{C-O} in Rh_xCO GSs show a ν_{C-O} reduction of the free CO from 7.7 to 8.6% in the range of the experimentally established[35−37,39] one.

As seen from Table 3, the CO stretching frequency of RhCO (2043 cm^{-1}) undergoes a decrease of only 22, 5, and 15 cm^{-1} in the Rh_2CO, Rh_3CO, and Rh_4CO ground states, respectively. These observations lead to the conclusion that the surrounding metal atoms do not influence significantly the CO stretching frequency, whatever topology of the metal arrangement is considered. Therefore, the linear CO bonding to rhodium is predominantly determined by the local CO−Rh interaction. This is also consistent with the ν_{C-O} = 2022 cm^{-1} measured for RhCO in solid neon,[10,11] which is near the metal surface CO adsorption frequency.[36]

The Rh−C stretching frequencies (ν_{Rh-C}) of the monocarbonyls are also given in Table 3. A pronounced dependence of ν_{Rh-C} on the electronic structure can be noted. Nevertheless, the GS Rh−C stretching frequencies fall in the range of the experimental ν_{Rh-C} reported for CO adsorption on Rh(100) (ν_{Rh-C} = 535 cm^{-1})[40] and Rh(311) (ν_{Rh-C} = 524 cm^{-1})[41] at low CO coverage.

TABLE 2: Geometrical Parameters and CO Stretching Frequencies for CO, RhCO, and $Rh(CO)_2$ from Different Levels of Theory[a]

system	method	r(Rh−C)	r(C−O)	∠(Rh−C−O)	ν_{C-O}	$\Delta\nu_{C-O}$
CO	B3LYP +DZVP		1.141		2191	
	B3LYP+LANL2(DZ)		1.128		2213	
	BP86+ LANL2(DZ)		1.140		2122	
	MRSDCI[b]		1.128		2260	
	LSD[c]		1.140		2163	
RhCO	B3LYP +DZVP	1.863	1.162	180.0	2039	152
	B3LYP+LANL2(DZ)	1.820	1.153	180.0	2043	170
	BP86+ LANL2(DZ)	1.791	1.171	179.3	1959	163
	MRSDCI[b]	1.839	1.146		2127	133
	LSD[c]	1.758	1.169		2037	126
$Rh(CO)_2$	B3LYP +DZVP	1.931	1.156	170.2, 100.2	2090, 2041	101
	B3LYP+LANL2(DZ)	1.895	1.145	170.0, 101.5	2099, 2035	114
	BP86+ LANL2(DZ)	1.865	1.162	168.7, 98.8	2006, 1949	116
	LSD[c]	1.832	1.161	177.1, 85.9	2074, 2013	89

[a] The bond distances (r) are in Å, bond angles are in degrees, and the vibrational frequencies (ν_{C-O}) are in cm^{-1}. For $Rh(CO)_2$, the second angle is the angle between C−Rh−C. $\Delta\nu_{C-O} = \nu_{C-O}$ (CO) − ν_{C-O} ($Rh(CO)_x$, $x = 1, 2$). [b] From ref 8. [c] From ref 7.

TABLE 3: B3LYP C−O (ν_{C-O}) and Rh−C (ν_{Rh-C}) Stretching Frequencies in cm^{-1} and Intensities (I_{C-O} and I_{Rh-C}) in km/mol for Rh_xCO Structures

system	spin	ν_{C-O}	I_{C-O}	ν_{Rh-C}	I_{Rh-C}
RhCO	1/2	2043	687	502	7
	3/2	2017	1404	347	15
Rh_2CO	0	2040	852	548	8
	1	2021	843	560	6
	2	2063	1060	447	16
Rh_2CO[a]	0	1908	577	450	2
	1	1883	537	445	0
Rh_3CO	1/2	2029	1166	492	30
	3/2	2038	912	569	13
	5/2	2033	1269	456	33
Rh_4CO[b]	0	2059	1126	488	14
Rh_4CO	0	2065	967	549	18
	1	2035	1250	472	21
	2	2028	1181	487	15

[a] CO adsorbed in bridge position. [b]Planar Rh_4CO structure.

TABLE 4: B3LYP C−O (ν_{C-O}) Symmetric and Asymmetric Stretching Frequencies and C−C Bending (ν_{C-C}) Frequencies in cm^{-1} and Intensities (I_{C-O} and I_{C-C}) in km/mol for $Rh_x(CO)_2$ Species

system	geometry[a]	ν_{C-O}	I_{C-O}	ν_{C-C}	I_{C-C}
$Rh(CO)_2$	1	2099	403	512	0
		2041	1315		
$Rh_4(CO)_2$	2	2094	960	480	33
		2043	2094		
OC−Rh_2−CO	3	2070	1004	412	1
		2027	462		
OC−Rh_4−CO	4	2071	1072	390	1
		2049	1179		
OC−Rh_4−CO	5	2075	1515	429	4
		2029	627		

[a] The geometry numbers refer to the corresponding $Rh_x(CO)_2$ structures drawn in Figure 2.

4.2. CO Stretching Frequencies of $Rh_x(CO)_2$. In Table 4 the computed vibrational features for the dicarbonyl species are presented. Considering first the dicarbonyls with the CO molecules bound to the single Rh-site (structure **1** and **2** in Figure 2), we note that both species give rise to almost equal symmetric (ν^s_{C-O}) and asymmetric (ν^a_{C-O}) CO stretching frequencies.

The presence of Rh gem-dicarbonyl species on the supported rhodium particles is well established by the appearance of two infrared bands in the 2000 to 2100 cm^{-1} range.[35,42,43] The symmetric−asymmetric splitting is reported to amount to 70 cm^{-1} for Rh/Al_2O_3[43] and Rh in zeolites.[35] Our values for the gem-dicarbonyls predict a 5.1% reduction for the free C−O stretching frequency, which is twice that found experimentally. The splitting between both stretching modes obtained by us is about 20 cm^{-1} smaller than the splitting indicated from the experiments on Rh/Al_2O_3[43] and Rh in zeolites.[35] As discussed earlier, our B3LYP results for $Rh(CO)_2$ fall in the same range as those reported in the previous theoretical studies.

Another fact that needs to be mentioned in this context is that the gem-dicarbonyl on the supported rhodium is usually assigned to the formation of $Rh^I(CO)_2$ as the sole surface species.[43−45] This understanding has prompted a series of theoretical studies on the spectroscopic constants of $Rh(CO)_2^+$ species,[6,7,9−11] reporting two possible stable structures, the linear ($^3\Delta$)[6,7,10,11] and the bent ($^1A_1$)[7,9] ones. The frequency of the bent $Rh(CO)_2^+$ computed here predicts a blue shift to 2245 cm^{-1}, which is in clear contradiction with the experimentally observed ν^s_{C-O} in the gem-dicarbonyl. This result, however, agrees very well with the previous theoretical studies despite that the level of theory is employed and the electronic structure for the bent $Rh(CO)_2^+$ is considered.[7,9,10] Indeed, for the less stable $^3B_2$ species we have found $\nu^s_{C-O} = 2261$ cm^{-1}. The splittings between both stretching components for the $^1A_1$ and $^3B_2$ electronic states are 49 and 27 cm^{-1}, respectively. If we look at the Mulliken net charge (q) of the cation carbonyls given in Table 1, it emerges that the q_{Rh} in $Rh(CO)_2^+$ is 0.49, in agreement with the other DFT data, and the 1+ charge is redistributed in the way that a significant amount ($q = 0.48$) goes to the carbon atoms. The general correlation between the increase of ν_{C-O} with the increase of the net rhodium charge from neutral to cation gem-dicarbonyl already was discussed by Zhou and Andrews.[11] Thus, one might expect an even bigger blue shift of ν^s_{C-O} if the charge of rhodium is 1+.

It is interesting to note that whereas the ν_{C-O} for the considered gas-phase monocarbonyls (Table 3) generally agree with the IR data[3−5,10,11,35−37,39] for supported rhodium monocarbonyls, there is an obvious discrepancy between the calculated ν^s_{C-O} in the gas-phase $Rh(CO)_2$ species and the IR data for the gem-dicarbonyl on the surfaces.[35,43−45] Therefore, one can conclude that the influence of the support on the formation of $Rh(CO)_2$ seems to be more pronounced than on the formation of the monocarbonyls. It is difficult to compare our B3LYP frequencies with the IR bands observed in the matrix isolation spectroscopy experiments[11] since in that study only an IR band at 2031 cm^{-1} is assigned to the asymmetric ν_{C-O} in the linear $Rh(CO)_2$ species.

The symmetric and asymmetric stretching frequencies of the dicarbonyls with two CO molecules bound linearly to two Rh sites (geometries **3**, **4**, and **5** in Figure 2) are summarized also

in Table 4. Again, a small dependence of ν^{s}_{C-O} with the metal cluster topology is established. Indeed, the Rh−Rh distance of interest in structure **4** is longer by 1 Å than that in OC−Rh_2−CO, but the ν^{s}_{C-O} are almost equal for both cases. As expected, the positions of the asymmetric components vary with the distance between the two metal centers. The dipole−dipole coupling interaction obviously decreases with the Rh−Rh distance in structure **4**, and therefore the symmetric−asymmetric splitting is found to be half of that in OC−Rh_2−CO. Furthermore, the obtained ν_{C-O} blue shift of about 50 cm^{-1} in going from Rh_xCO to OC−Rh_x−CO clusters is consistent with the experimentally observed ν_{C-O} shift as a function of the CO coverage,[41] and therefore the small OC−Rh_x−CO species can be appropriate models for the CO−Rh interaction approaching saturation.

As already mentioned, the prompting force for the current theoretical study was the very recent experimental work[5] dealing with subnanometer size rhodium particles deposited on an ultrathin alumina film.[1−3] To gain insight into the morphology of these particles, the infrared (IR) features of adsorbed CO were examined using IRA spectroscopy.[3−5] The infrared spectrum taken from a Rh deposit with an average particle size below 5 atoms saturated with CO at low temperatures resulted in a series of sharp bands with low halfwidth. This points to the presence of uniform isolated $Rh_x(CO)_y$ species. The positions of these IR bands together with our B3LYP ν_{C-O} values of some selected monocarbonyls and dicarbonyls are drawn in Figure 3a. In the same figure the positions of the experimental and B3LYP ν_{C-O} value of free CO are also reported.

The bands observed at 2117 and 2087 cm^{-1} are identified by isotopic mixture experiments (mixture of ^{12}CO and ^{13}CO)[3−5] to originate from species containing two, and more than two, CO molecules, respectively. The band at 1999 cm^{-1} is probably due to the adsorption of a single CO molecule on Rh_x aggregates. Note that because of the surface selection rule the asymmetric components of $Rh(CO)_2$ species cannot be observed.[3−5] As pointed out earlier, the B3LYP values of ν_{C-O} in Rh_xCO GSs show a ν_{C-O} reduction ranging from 7.7 to 8.6%, which is in reasonable agreement with the value of 6.7% indicated by the experiments under discussion. Schematically, the intensity variation of the IR bands with ^{12}CO content in the ^{12}CO −^{13}CO mixture is shown in Figure 3b. Our B3LYP ν_{C-O} values of $Rh(^{12}CO)_2$, $Rh(^{12}CO)(^{13}CO)$, $Rh(^{13}CO)_2$, $Rh^{12}CO$, and $Rh^{13}CO$ are designated in the same figure. These results confirm the observed downshifts of 16 cm^{-1} in $Rh(^{12}CO)(^{13}CO)$ and of 50 cm^{-1} in $Rh(^{13}CO)_2$ with respect to ν_{C-O} in $Rh(^{12}CO)_2$, and those of 46 cm^{-1} in $Rh^{13}CO$ relative to $Rh^{12}CO$.

Furthermore, the computed shift of 30 cm^{-1} between the bands due to the $Rh(CO)_2$ and OC−Rh_2−CO coincides with the shift between the bands at 2117 and 2087 cm^{-1}. However, the evolution of the band at 2087 cm^{-1} with isotopic composition suggests the presence of $Rh_x(CO)_y$ with $y > 2$, since this band vanishes completely upon admixture of 33% ^{13}CO. For this reason a $Rh(CO)_3$ cluster has been considered. Our computations yield a T-shaped structure, in line with the BP86 calculations of Zhou and Andrews,[10,11] and a symmetric frequency of 2116 cm^{-1}, i.e., 17 cm^{-1} higher than ν^{s}_{C-O} in $Rh(CO)_2$. The frequency order is well reproduced within the DFT based approaches[33,34] and thus the presence of carbonyls with more than two CO molecules bound to the single rhodium center can be ruled out. The B3LYP optimization of the gas-phase $Rh_x(CO)_y$ ($x = 2-4$; $y = 3,4$) structures did not give any minimal geometry that can be postulated on the surface under these experimental circumstances.

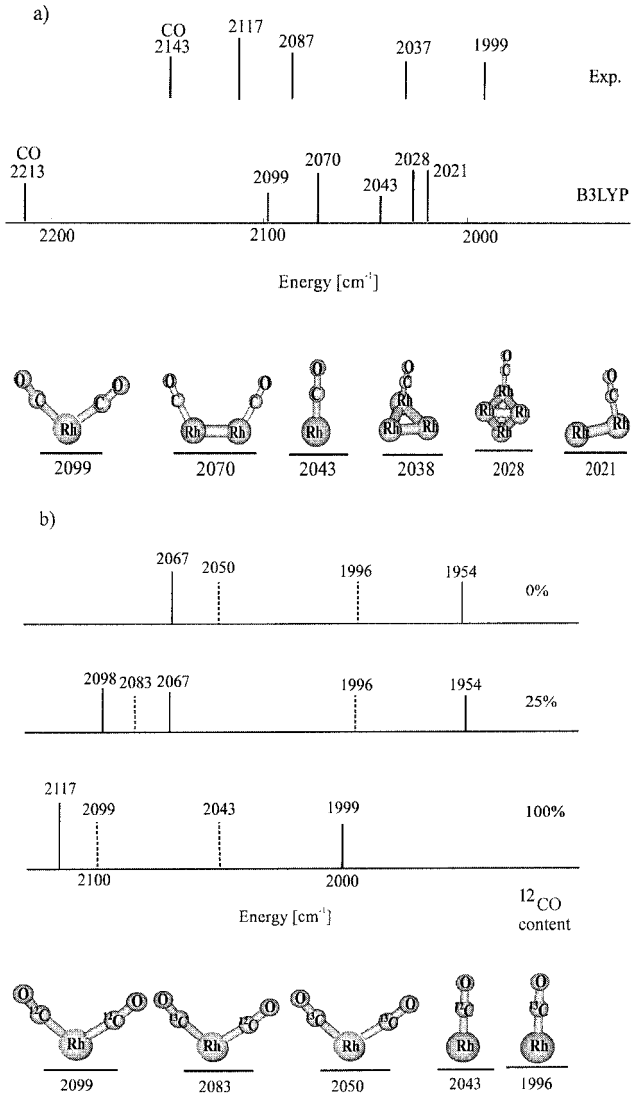

Figure 3. (a) Experimental and B3LYP-vibrational stretching frequencies of some selected $(CO)_{1,2}/Rh_x$ clusters. The experimental date are taken from ref 5. The experimental and B3LYP vibrational stretching frequencies of the free CO are also reported. (b) Vibrational stretching frequencies from the isotopic mixture experiment (^{12}CO and ^{13}CO) and B3LYP-vibrational stretching frequencies for $Rh(^{12}CO)_2$, $Rh(^{12}CO)(^{13}CO)$, $Rh(^{13}CO)_2$, $Rh^{12}CO$, and $Rh^{13}CO$. The dashed lines denote the B3LYP frequencies.

Finally, let us discuss the origin of the IR band at 2117 cm^{-1} (Figure 3a). The experimental evidences[3−5] pointed to a gem-dicarbonyl responsible for this signal. The computed reduction for the free ν_{CO} of 5.2% in $Rh(CO)_2$ and 5.0% in $Rh_4(CO)_2$ is higher by 3% roughly than the experimental value. So, as mentioned above, the support effect on the binding of two CO molecules to the single Rh site appears to be somewhat stronger than on the formation of the linear RhCO. To understand better the reasons for the latter result, further calculations accounting for the alumina support are under way.

5. Bonding Analysis

The nature of the adsorption bond between CO and d-metal surfaces is conventionally understood in terms of the 5σ CO donation to the metal associated with a back-donation to the empty 2π* CO orbital.[46] The great variety of the theoretical studies corroborates this overall description, although further analyses have involved the Pauli repulsion[47] and the balance

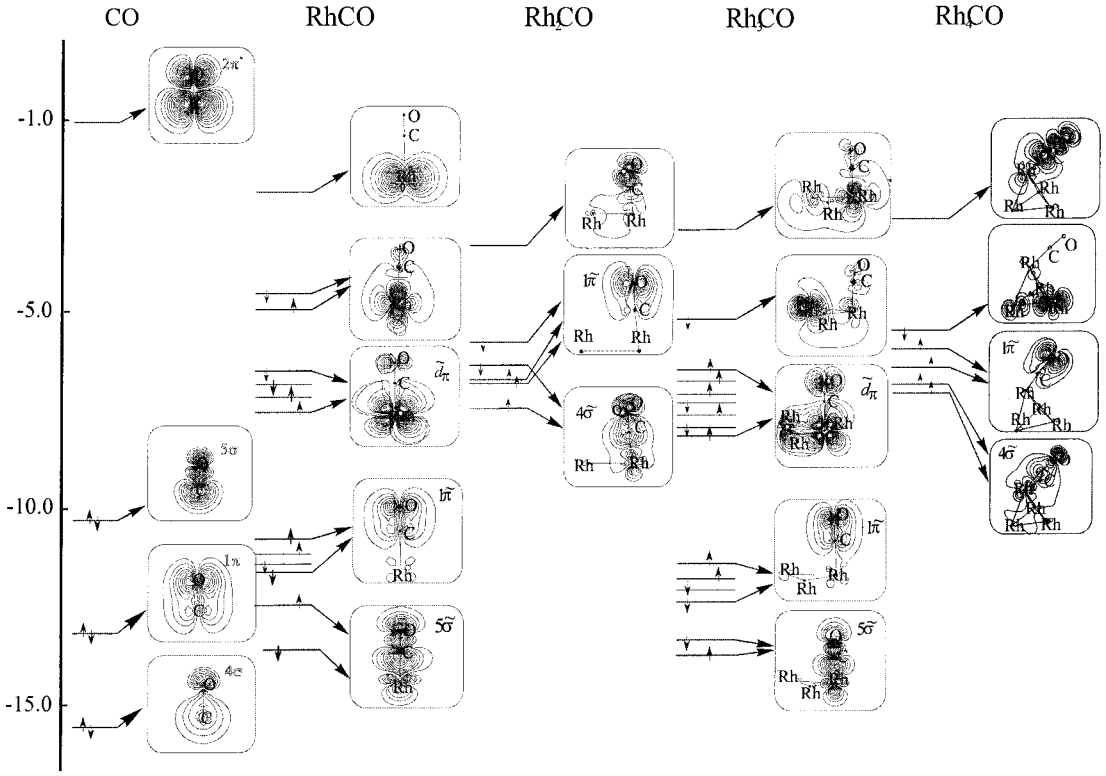

Figure 4. Contour plots of molecular orbitals with predominantly C and O character in the Rh_xCO species from B3LYP computations. LUMO and HOMO for each molecule are also plotted.

between π-bonding and σ-repulsion in the CO bonding mechanism.[48−50] In this section we are mainly going to analyze the nature of the molecular orbitals (MOs) in the monocarbonyls with the aim to describe how the magnetism and the number of atoms in the small rhodium clusters affect the C−O bond.

Starting with the analysis of the molecular contour plots of the most interesting MOs for the Rh_xCO ground states, reported in Figure 4, we note that the CO interaction with the rhodium atom and trimer yields orbitals that differ remarkably from those for Rh_2CO and Rh_4CO. The evolution of the free CO electronic states in RhCO and Rh_3CO consists of the formation of new π type valence orbitals ($\tilde{d}_\pi$) composed by the metal d_π electrons and the oxygen lone pair. There are other π type orbitals ($1\tilde{\pi}$) having the symmetry and character close to the 1π in free CO. The orbitals of σ-symmetry ($5\tilde{\sigma}$) with character and shape resembling those of 5σ in free CO lie below the 1π. Very recently, a similar MO picture has been reported for CO binding on Ni(100) and Cu(100) surfaces using X-ray emission spectroscopy and DFT calculations.[49,50] The MOs with predominantly metal−metal bond character in Rh_3CO occupy the space between the highest occupied molecular orbital (HOMO) and $\tilde{d}_\pi$ and between the $\tilde{d}_\pi$ and $1\tilde{\pi}$ orbitals. Hence, the role of the metal−metal bond seems to be in preserving the energies of $\tilde{d}_\pi$ and $1\tilde{\pi}$ close to those of their counterparts in RhCO.

The molecular orbital coefficients for the other less stable states of Rh_3CO (doublet and sextet) are qualitatively very similar to the most stable quartet one. The $2\pi^*$ electronic state becomes the highest singly occupied orbital only in the $^4\Delta$ RhCO structure. The $^4\Delta$ state is the only example among the series of $Rh_x(CO)_y$ clusters of the metal back-donation to the $2\pi^*$ CO orbital that corroborates also the inverse relation between the extent of π back-donation and the shift in CO stretching frequency.

The MO contour plots of the triplet and quintet Rh_2CO and Rh_4CO ground-state structures show a quite different picture compared to the MOs of the carbonyls with an odd number of rhodium atoms. Indeed, the $\tilde{d}_\pi$ orbital is no more formed and instead a dramatic destabilization of 1π and 4σ is obtained. The occupied electronic states with predominantly metal character fill the space below the $1\tilde{\pi}$ and $4\tilde{\sigma}$ orbitals. Moreover, an occupied orbital with a $5\tilde{\sigma}$ character is not identified. The $4\tilde{\sigma}$ is polarized toward the carbon atom which facilitates its overlap to the d_σ rhodium electrons.

The less stable Rh_2CO (singlet) and the Rh_4CO clusters form molecular orbitals, which closely resemble those of the monocarbonyls with an odd number of Rh atoms. Most probably, this fact reflects the increase in the CO stretching frequency in going from ground to the excited Rh_2CO and Rh_4CO states. It is surprising that the MOs in the quintet Rh_2CO are very similar to those in the triplet (GS) structure, despite the remarkable ν_{C-O} differences for both spin-states (see Table 3). Nevertheless, the increased spin-polarization in the quintet structure yields a shorter C−O bond (see Figure 1), which may be the reason for the 40 cm^{-1} blue shift relative to the triplet GS one.

The above analysis reveals that it is difficult to rationalize the C−O bond evolution in the series of monocarbonyls only within the frontier 5σ-donation-$2\pi^*$-back-donation theory. The participation of the low-lying 1π and 4σ orbitals is evident. Moreover, except for the quartet RhCO molecule, the $2\pi^*$ states are determined to lie higher than the lowest unoccupied molecular orbitals (LUMOs). Even if one associates the stabilization of $5\tilde{\sigma}$ in RhCO and Rh_3CO GSs with the σ-donation to the metal atoms and consequently the formation of the $\tilde{d}_\pi$ orbitals with the back-donation from the metal, the CO interaction with the dimer and tetramer cannot be accommodated in such a framework. In the latter case, the MO picture suggests that the C−O bond weakness is rather due solely to the σ-donation to the rhodium atoms, which in turn leads to an increase in the electronic repulsion within the entire compound and thus to a significant destabilization of 1π and 4σ orbitals.

TABLE 5: Natural Electron Configuration for the Ground State $Rh_x(CO)_y$ from the B3LYP Natural Bond Order Analysis

	C		O		Rh[a]			
system	2s	2p	2s	2p	5s	4d	5p	5d
CO	1.64	1.83	1.73	4.73				
RhCO	1.28	2.22	1.71	4.76	0.30	8.66		
Rh_2CO	0.97	0.49	1.80	3.98	0.44	9.95	0.14	0.19
Rh_3CO	1.16	2.23	1.70	4.77	0.56	8.56		
Rh_4CO	0.61	0.30	1.79	2.45	0.24	9.92	0.09	0.27
$Rh(CO)_2$	1.45	2.34	1.70	4.68	0.77	7.55	0.09	0.01
$OC-Rh_2-CO$	1.18	2.20	1.70	4.75	0.48	8.61		

[a] Natural electron configuration of rhodium atom bound to the CO molecule.

The above bonding schemes are supported also by the natural electron configuration (NEC) values presented in Table 5 for the ground state monocarbonyl arrangements. The hybridization between outer s and d electrons of the rhodium atom(s) facilitates a promotion of a fraction of an electron from 5s to 4d states, and the resulting 5s occupancy does not vary significantly within the Rh_xCO series. For RhCO GS, we note the very good agreement between our NEC values and the NEC values from MRSDCI[8] computations. In the RhCO and Rh_3CO clusters the resulting electronic transfer between rhodium and CO molecules is almost negligible. By contrast, the CO interaction with the Rh_2 and Rh_4 is accompanied by the electronic transfer from the CO molecule to the metal d shell.

To summarize, let us note that these completely different bonding schemes of CO to the rhodium atom and trimer on one hand and to the rhodium dimer and tetramer on the other hand lead to the ν_{C-O} values varying only by 20 cm^{-1}. So, it seems to be far from straightforward to establish a general correlation between the CO bonding mechanism in the carbonylated rhodium clusters and the CO vibrational stretching frequency. On the basis of our calculations we can only conclude that the extent of the factors as σ-donation, π-back-donation, electron rearrangements, and electrostatic interactions depends on the particular electronic configuration and magnetic characteristics that are associated with the geometrical structures as well.

The molecular orbital coefficients for the $Rh_x(CO)_2$ and $OC-Rh_x-CO$ species reveal the formation of $\tilde{d}_\pi$, $5\tilde{\sigma}$, and $1\tilde{\pi}$ orbitals, which do not differ significantly in their shape and character from the MOs in the RhCO and Rh_3CO. Nevertheless, an increased polarization of the $1\tilde{\pi}$ and $5\tilde{\sigma}$ orbitals toward the carbon site is noted. This gives rise to bonding orbitals with higher metals participation relative to the CO bonding in the monocarbonyls. We also mention the appearance of a CO−CO bonding orbital of σ-type between the $5\tilde{\sigma}$ states of each CO molecule in the case of $Rh(CO)_2$ and $Rh_4(CO)_2$.

For $OC-Rh_x-CO$ species, a bonding orbital between both carbon monoxide molecules is not formed. Therefore, a direct molecular orbital CO−CO interaction does not contribute to the ν_{C-O} shifts ranging from 50 to 75 cm^{-1} relative to the ν_{C-O} in the rhodium monocarbonyls.

6. Conclusion

B3LYP-spectroscopic constants of fully optimized geometrical structures of $Rh_x(CO)_y$ ($x \leq 4$, $y \leq 2$) species have been presented in this work. The results can be summarized as follows.

Small rhodium carbonyls exhibit nonzero magnetic moments as do small rhodium clusters. The interaction of CO with the single atom and dimer is clearly predicted to reduce the Rh and Rh_2 ground state magnetic moments. The presence of a second CO molecule leads to paramagnetic $Rh(CO)_2$ and $Rh_2(CO)_2$ structures.

The carbon monoxide vibrational stretching frequency is slightly influenced by rhodium cluster topology but depends more strongly on the electronic configuration. Therefore, precisely established ground state structures with correctly obtained relaxed geometries of the entire cluster are needed in order to achieve correct harmonic frequencies.

The symmetric CO stretching frequencies for $Rh_x(CO)_2$ species are also sligthly affected by the number of Rh atoms. The asymmetric components of the CO stretching frequencies are, however, more specific for the $Rh_x(CO)_2$ geometries.

The ν_{C-O} for the Rh_xCO ground-state generally agree with the experimental data, while the value of the symmetric ν_{C-O} for the gem-dicarbonyl is more strongly influenced by the support. To give more insight into this problem, further calculations accounting for the influence of an alumina substrate are under way.

The detailed MO analysis suggests that the CO bonding mechanism, and thus the CO bond strength, is very sensitive to the particular electron distribution, e.g., the spin-states and the initial occupations of the Rh 5s electronic states. Moreover, for Rh_xCO species, σ-donation, π-back-donation, electron redistribution, and electrostatic interactions may differ significantly between molecules containing an even number of Rh atoms and those containing an odd number of Rh atoms.

Acknowledgment. T.M. expresses her gratitude to the Alexander von Humboldt Foundation for a research fellowship.

References and Notes

(1) Jaeger, R. M.; Kuhlenbeck, H.; Freund, H.-J.; Wuttig, M.; Hoffmann, W.; Francy, R.; Ibach, H. *Surf. Sci.* **1994**, *318*, 61.
(2) Freund, H.-J. *Angew. Chem., Int. Ed. Engl.* **1997**, *36*, 452.
(3) Frank, M.; Kühnemuth, R.; Bäumer, M.; Freund, H.-J. *Surf. Sci.* **2000**, *454−456*, 968.
(4) Frank, M.; Kühnemuth, R.; Bäumer, M.; Freund, H.-J. *Surf. Sci.* **1999**, *427−428*, 288.
(5) Frank, M.; Bäumer, M.; Kühnemuth, R.; Freund, H.-J. *J. Phys. Chem. B* **2001**, *105*, 8569.
(6) Barnes, L. A.; Rosi, M.; Bauschlicher, C. W., Jr. *J. Chem. Phys.* **1990**, *93*, 609.
(7) Papai, I.; Goursot, A.; St-Amanat, A.; Salahub, D. R. *Theor. Chim. Acta* **1992**, *84*, 217.
(8) Dai, D.; Balasubramanian, K. *J. Chem. Phys.* **1994**, *101*, 2184.
(9) McKee, M. L.; Worley, S. D. *J. Phys. Chem. A* **1997**, *101*, 5600.
(10) Zhou, M.; Andrews, L. *J. Phys. Chem. A* **1999**, *103*, 7773.
(11) Zhou, M.; Andrews, L. *J. Am. Chem. Soc.* **1999**, *121*, 9171.
(12) Koutecky, J.; Pacchioni, G.; Fantucci, P. *Chem. Phys.* **1985**, *99*, 87.
(13) Blyholder, G. *J. Mol. Catal. A: Chem.* **1997**, *119*, 11.
(14) Goursot, A.; Papai, I.; Salahub, D. R. *J. Am. Chem. Soc.* **1992**, *114*, 7452.
(15) Gingerich, K. A.; Cocke, D. L. *J. Chem. Soc., Chem. Commun.* **1972**, *1*, 536.
(16) Wang, H.; Haouari, H.; Craig, R.; Liu, Y.; Lombardi, J. R.; Lindsay, D. M. *J. Chem. Phys.* **1997**, *106*, 2101.
(17) Cox, A. J.; Louderback, J. G.; Apsel, S. E.; Bloomfield, L. A. *Phys. Rev. B* **1994**, *49*, 12295.
(18) Van Zee, R. J.; Hamrick, Y. M.; Li, S.; Weltner, W., Jr. *Chem. Phys. Lett.* **1992**, *195*, 214.
(19) Chien, C.-H.; Blaisten-Barojas, E.; Pederson, M. R. *Phys. Rev. A* **1998**, *58*, 2196.
(20) Chien, C.-H.; Blaisten-Barojas, E.; Pederson, M. R. *J. Chem. Phys.* **2000**, *112*, 2301.
(21) Lacaze-Dufaure, C.; Mineva, T.; Russo, N. *Int. J. Quantum Chem.* **2001**, *85*, 162.
(22) Becke, A. D. *J. Chem. Phys.* **1993**, *98*, 5648.
(23) Lee, C.; Yang, W.; Parr, R. G. *Phys. Rev. B* **1988**, *37*, 785.
(24) Hay, P. J.; Wadt, W. R. *J. Chem. Phys.* **1985**, *82*, 270. Hay, P. J.; Wadt, W. R. *J. Chem. Phys.* **1985**, *82*, 299. Wadt, W. R.; Hay, P. J. *J. Chem. Phys.* **1985**, *82*, 284.

(25) McLean, A. D.; Chandler, G. S. *J. Chem. Phys.* **1980**, *72*, 5639. Krishnan, R.; Binkley, J. S.; Seeger, R.; Pople, J. A. *J. Chem. Phys.* **1980**, *72*, 650.

(26) Peng, C.; Ayala, P. Y.; Schlegel, H. B.; Frisch, M. J. *J. Comput. Chem.* **1996**, *17*, 49.

(27) Godbout, N.; Salahub, D. R.; Andzelm, J.; Wimmer, E. *Can. J. Phys.* **1992**, *70*, 560.

(28) Cheeseman, J. R.; Frisch, M. J.; Devlin, F. J.; Stephens, P. J. *Chem. Phys. Lett.* **1996**, *252*, 211.

(29) Perdew, J. P. *Phys. Rev. B* **1986**, *33*, 8822. Becke, A. D. *J. Chem. Phys.* **1993**, *98*, 5648.

(30) Frisch, M. J.; Trucks, G. W.; Schlegel, H. B.; Gill, P. M. W.; Johnson, B. G.; Robb, M. A.; Cheesman, J. R.; Keith, T. A.; Petersson, G. A.; Montgomery, J. A.; Raghavachari, K.; Al-Laham, M. A.; Zakrzewski, V. G.; Ortiz, J. V.; Foresman, J. B.; Croslowski, J.; Stefanov, B. B.; Nanayakkara, A.; Challacombe, M.; Peng, C. Y.; Ayala, P. Y.; Chen, W.; Wong, M. W.; Andres, J. L:, Replogle, E. S.; Gomperts, R.; Martin, R. L.; Fox, D. J.; Binkley, J. S.; Defrees, D. J.; Baker, J.; Stewart, J. P.; Head-Gordon, M.; Gonzales, C.; Pople, J. A. *Gaussian 94* (Revision A.1) Gaussian, Inc.: Pittsburgh, PA, 1995.

(31) Moore, C. E. Ionization Potential and Ionization Limits from the Analysis of Optical Spectra in *National Bureau of Standards Reference Data Series*; National Bureau of Standards (U.S.) Circ. No 34; U.S. Government Printing Office: Washington, DC., 1970.

(32) Pacchioni, G.; Rosch, N. *Acc. Chem. Res.* **1995**, *28*, 390.

(33) Chermette, H. *Coord. Chem. Rev.* **1998**, *178*−*180*, 699 and references therein.

(34) Wong, M. W. *Chem. Phys. Lett.* **1996**, *256*, 391.

(35) Conners, L.; Hollis, T.; Johnson, D. A.; Blyholder, G. *J. Phys. Chem. B* **1998**, *102*, 10112.

(36) Leung, L.-W. H.; He, J.-W.; Goodman, D. W. *J. Chem. Phys.* **1990**, *93*, 8328.

(37) de Jong, A. M.; Niemantsverdriet, J. W. *J. Chem. Phys.* **1994**, *101*, 10126.

(38) Herzberg, G. *Molecular Spectra and Molecular Structure*; 2nd ed.; Van Nostrand Reinhold: New York, 1950; Vol. 1.

(39) Wei, D. H.; Skelton, D. C.; Kevan, S. D. *Surf. Sci.* **1997**, *381*, 49.

(40) Dubois, L. H. *J. Chem. Phys.* **1982**, *77*, 5228.

(41) Batteas, J. D.; Gardin, D. E.; Van Hove, M. A.; Somorjai, G. A. *Surf. Sci.* **1993**, *297*, 11.

(42) Yang, A. C.; Garland, C. W. *J. Phys. Chem.* **1957**, *61*, 1504.

(43) Yates, J. T., Jr.; Kolasinski, K. *J. Chem. Phys.* **1983**, *79*, 1026.

(44) Primet, M. *J. Chem. Soc., Faraday Trans. 1* **1978**, *74*, 2570.

(45) Knözinger, H.; Thorton, E. W.; Wolf, M. *J. Chem. Soc., Faraday Trans. 1* **1979**, *75*, 1888.

(46) Blyholder, G. J. *J. Phys. Chem.* **1964**, *68*, 2772.

(47) Bagus, P. S.; Pacchioni, G. *Surf. Sci.* **1990**, *236*, 233.

(48) Föhlisch, A.; Nyberg, M.; Bennich, P.; Triguero, L.; Hasselström, J.; Karis, O.; Petterson, L. G. M.; Nilsson, A. *J. Chem. Phys.* **2000**, *112*, 1946.

(49) Föhlisch, A.; Nyberg, M.; Hasselström, J.; Karis, O.; Petterson, L. G. M.; Nilsson, A. *Phys. Rev. Lett.* **2000**, *85*, 3309.

(50) Föhlisch, A.; Nyberg, M.; Bennich, P.; Triguero, L.; Hasselström, J.; Karis, O.; Petterson, L. G. M.; Nilsson, A. *J. Chem. Phys*. **2000**, *112*, 1946.

(51) Reed, A. E.; Curtiss, L. A.; Weinhold, F. *Chem. Rev.* **1988**, *88*, 899 and references therein.